

Role of Procoagulant Lipids in Human Prothrombin Activation. 1. Prothrombin Activation by Factor X_a in the Absence of Factor V_a and in the Absence and Presence of Membranes[†]

Jogin R. Wu,[‡] Chaoming Zhou,[§] Rinku Majumder, Daniel D. Powers,^{||} Gabriel Weinreb, and Barry R. Lentz^{*}

Department of Biochemistry and Biophysics, CB 7260, University of North Carolina at Chapel Hill, Chapel Hill, North Carolina 27599-7260

Received August 20, 2001; Revised Manuscript Received October 25, 2001

ABSTRACT: Activation of prothrombin by factor X_a requires proteolysis of two bonds and is commonly assumed to occur via two parallel, sequential pathways. Hydrolysis of Arg³²²–Ile³²³ produces meizothrombin (MzII_a) as an intermediate, while hydrolysis of Arg²⁷³–Thr²⁷⁴ produces prethrombin 2–fragment 1.2 (Pre2–F1.2). Activation by human factor X_a of human prothrombin was examined in the absence of factor V_a and in the absence and presence of bovine phosphatidylserine (PS)/palmitoylphosphatidylcholine (25:75) membranes. Four sets of data were collected: fluorescence of an active site probe (DAPA) was sensitive to thrombin, MzII_a, and Pre2–F1.2; a synthetic substrate (S-2238) detected thrombin or MzII_a active site formation; and SDS–PAGE detected both intermediates and thrombin. The fluorescence data provided an internal check on the active site and SDS–PAGE measurements. Kinetic constants for conversion of intermediates to thrombin were measured directly in the absence of membranes. Both MzII_a and Pre2–F1.2 were consumed rapidly in the presence of membranes, so kinetic constants for these reactions had to be estimated as adjustable parameters by fitting three data sets (thrombin and MzII_a active site formation and Pre2 appearance) simultaneously to the parallel-sequential model. In the absence of membranes, this model successfully described the data and yielded a rate constant, 44 M⁻¹ s⁻¹, for the rate of MzII_a formation. By contrast, the parallel-sequential model could not describe prothrombin activation in the presence of optimal concentrations of PS-containing membranes without assuming that a pathway existed for converting prothrombin directly to thrombin without release from the membrane–enzyme complex. The data suggest that PS membranes (1) regulate factor X_a, (2) alter the substrate specificity of factor X_a to favor the meizothrombin intermediate, and (3) “channel” intermediate (MzII_a or Pre2–F1.2) back to the active site of factor X_a for rapid conversion to thrombin.

The final step in the blood coagulation cascade involves the activation of prothrombin to thrombin, which is the central enzyme of the coagulation system (13). This activation occurs most readily in the presence of a fully assembled enzyme complex, called prothrombinase (16, 32, 37), which consists of blood coagulation factors X_a (a serine protease) and V_a (a cofactor), Ca²⁺, and negatively charged phospholipid membranes derived from stimulated platelets (39).

Proteolytic activation of prothrombin gives rise to at least two different intermediate products depending upon which of two peptide bonds, Arg²⁷³–Thr²⁷⁴ or Arg³²²–Ile³²³, is cleaved first (bonds 2 and 1 in Figure 1). We refer to activation via these two possible intermediates as a “parallel-sequential activation mechanism”. In the presence of factor V_a and phospholipid, meizothrombin (MzII_a;¹ bond Arg³²²–Ile³²³ cleavage; see Figure 1) has been detected (21, 38), while in the absence of factor V_a or phospholipid, prethrombin 2 (Pre2;¹ bond Arg²⁷³–Thr²⁷⁴ cleavage; see Figure 1) has been

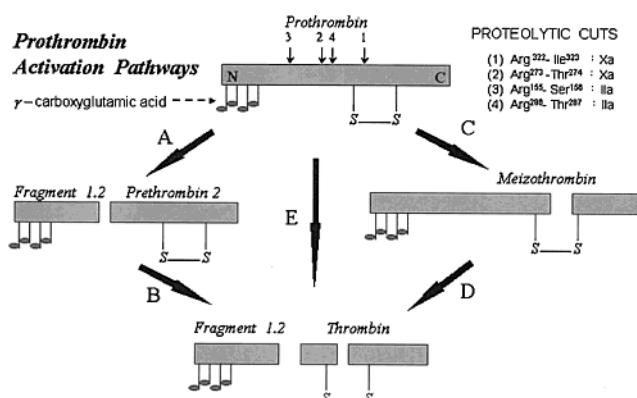


FIGURE 1: Schematic representation of human prothrombin activation. Prothrombin consists of a membrane-binding N-terminal domain (fragment 1.2) and a C-terminal catalytic domain (prethrombin 2). γ -Carboxylated glutamic acid residues at the C terminus are needed for membrane binding. Two peptide bonds [sites 2 (Arg²⁷³–Thr²⁷⁴) and 4 (Arg³²²–Ile³²³)] must be hydrolyzed by factor X_a in order to activate prothrombin. This creates two possible pathways of activation (A and B, C and D) and two possible released intermediates: Pre2 and MzII_a. A third possible pathway of activation is envisioned (E) in which no intermediate is released.

reported to accumulate (12, 37). These observations, along with data on the rate of intermediate conversion to thrombin,

[†] Supported by USPHS Grant HL45916.

^{*} To whom correspondence and requests for reprints should be addressed at UNC-CH. E-mail: uncbri@med.unc.edu.

[‡] Current address: Duke University, Durham, NC.

[§] Current address: Biochemistry Department, University of Otago, Dunedin, New Zealand.

^{||} Current address: Alcatel Corp., Inc., Raleigh, NC.

led to the proposal that the presence of factor V_a and a procoagulant membrane switches activation to proceed via the $MzII_a$ intermediate, although significant $MzII_a$ intermediate can be detected only at high prothrombin concentration (22, 30, 36). However, this conclusion remains tentative. Even in the absence of both phospholipid and membrane, $MzII_a$ was detected as an intermediate when bovine prothrombin 1 (prothrombin minus N-terminal Glu and epidermal growth factor-like domains) was used as the substrate (4).

What we do know is that, in the presence of factor V_a and phospholipid, the rates at which Pre2 plus fragment 1.2 or $MzII_a$ can be activated to thrombin are about the same (21, 30). Thus, the pathway of activation must be determined by the first proteolytic step. Unfortunately, we know very little about the rates of the first two possible steps of activation, since the intermediates are consumed at rates comparable to those at which they are produced. Since prothrombin and $MzII_a$ assume very different conformations on phosphatidylserine (PS)¹-containing membranes (7), we cannot assume that Arg²⁷³–Thr²⁷⁴ is cut at the same rate in prothrombin as in $MzII_a$ or that Arg³²²–Ile³²³ is cut in prothrombin at the rate at which Pre2–F1.2 is activated. Without estimates of the rates of prothrombin activation to the two possible intermediates, one cannot even test whether the commonly accepted parallel-sequential kinetic model provides an appropriate description of the rates of appearance of activation intermediates and products when prothrombin is activated.

Even if it is true that activation proceeds via the $MzII_a$ intermediate according to the parallel-sequential model, we still do not know whether it is factor V_a or the membrane surface, or a combination of both, that directs factor X_a to attack Arg³²²–Ile³²³ in prothrombin in preference to Arg²⁷³–Thr²⁷⁴. There is evidence that factor X_a is altered by its interaction with PS and thus that the membrane may play a significant role in determining the pathway of activation (15, 20, 44). Although this interaction clearly enhances the rate of prothrombin activation (20), we do not know the mechanistic consequences of these alterations in factor X_a conformation by PS-containing membranes. Most papers that have addressed the issue of the pathway of prothrombin activation included membranes along with factor V_a (21, 32), meaning that the separate effects of membranes and factor V_a could not be distinguished. Measurements taken over a range of factor V_a concentrations in the absence of phospholipid membranes have been extrapolated, using a thermodynamic and kinetic model, to conclude that factor V_a and not the membrane is responsible for the enhancement of Arg³²²–Ile³²³ cleavage in Pre2 as compared to Arg²⁷³–Thr²⁷⁴ cleavage in $MzII_a$ (3). No similar analysis of pro-

thrombin activation has been made in the presence of membranes but absence of factor V_a .

The aim of this paper is to define better the separate roles of membranes and factor V_a in determining the pathway of prothrombin activation by answering three questions. First, we ask whether PS membranes affect differently factor X_a 's activity toward the Arg²⁷³–Thr²⁷⁴ or the Arg³²²–Ile³²³ bond of prothrombin? In addition, does a membrane surface aid activation in some other way, such as by directing substrate or a specific intermediate to the membrane-bound enzyme? Finally, can the parallel-sequential model account for the observed appearance and disappearance of activation intermediates and thrombin in the absence or presence of procoagulant membranes?

To answer these questions, we determined the rates of all four single proteolytic steps (A–D in Figure 1) that are presumed to contribute to prothrombin activation in the absence and presence of four concentrations of PS-containing membranes. A determination of these rates in the absence of membranes has already been reported in the context of the parallel-sequential model for the bovine enzyme (4), and we have redetermined these rates for human prothrombin activation to establish a baseline of human factor X_a behavior and to show that the parallel-sequential model provides a good description of prothrombin activation in the absence of membranes. By contrast, the parallel-sequential model could not describe the kinetics of prothrombin activation in the presence of optimal concentrations of PS-containing membranes. However, if we assumed that some fraction of prothrombin converted directly to thrombin by pathway E in Figure 1 (i.e., one or both intermediates were "channeled" without being released from the enzyme), the resulting three-pathway model accounted for the data. The kinetic constants that derived from this analysis of our data showed that the greatest effect of a PS-containing membrane was on proteolysis of the Arg³²²–Ile³²³ bond by factor X_a .

EXPERIMENTAL PROCEDURES

Materials

Bovine brain phosphatidylserine (PS)¹ and 1-palmitoyl-2-oleoyl-3-*sn*-phosphatidylcholine (POPC)¹ were purchased from Avanti Polar Lipids Inc. (Alabaster, AL). The factor X_a -specific substrate *N*-2-benzyloxycarbonyl-D-arginyl-L-arginine *p*-nitroanilide dihydrochloride (S-2765)¹ and thrombin (IIa)¹-specific substrate H-D-phenylalanyl-L-pipecolyl-L-arginine *p*-nitroanilide dihydrochloride (S-2238)¹ were obtained from AB Kabi Diagnostica (Molndal, Sweden). Dansylarginine-*N*-(3-ethyl-1,5-pentanedyl)amide (DAPA)¹ was synthesized and purified according to literature reports (25, 31). Purified Russel's viper venom factor X activator was obtained from Hematologic Technologies Inc. (Essex Junction, VT). *Echis carinatus* venom (ECV)¹ and ecarin, soybean trypsin inhibitor, and Sephadex C-50 DEAE Tris-acryl Plus-M weakly basic anion exchanger were purchased from Sigma (St. Louis, MO). Iodo-beads were purchased from Pierce Chemical Co. (Rockford, IL). Na¹²⁵I (100 mCi/mL), contained in a solution of 0.1 N NaOH, was obtained from ICN Pharmaceutical, Inc. (Irvine, CA). SP-Sephadex C-50 was obtained from Pharmacia Fine Chemicals (Piscataway, NJ). D-Phenylalanyl-L-prolyl-L-arginine chloromethyl ketone (PPACK)¹ was purchased from Bachem Bioscience

¹ Abbreviations: II, prothrombin; Pre2, prothrombin 2; $MzII_a$, meizothrombin; II₂, thrombin; DAPA, dansylarginine-*N*-(3-ethyl-1,5-pentanedyl)amide; ECV, *Echis carinatus* venom; Hepes, 4-(hydroxyethyl)-1-piperazineethanesulfonic acid; Na₂EDTA, disodium ethylenediaminetetraacetate; PEG 8000, poly(ethylene glycol); PMSF, phenylmethanesulfonyl fluoride; PPACK, D-phenylalanylprolyl-L-arginine chloromethyl ketone; S-2765, benzyloxycarbonylarginylarginine *p*-nitroanilide (synthetic substrate for factor X_a); S-2238, phenylalanylpipecolylarginine *p*-nitroanilide (synthetic substrate for thrombin); SDS–PAGE, sodium dodecyl sulfate–polyacrylamide gel electrophoresis; Tris, tris(hydroxymethyl)aminomethane; PS, phosphatidylserine (bovine brain in this study); POPC, 1-palmitoyl-2-oleoyl-3-*sn*-phosphatidylcholine; LUV, large unilamellar vesicle.

Inc. (Philadelphia, PA). All other chemicals were ACS reagent grade; all solvents were HPLC grade.

Methods

Protein and Peptide Isolation. Human plasma for protein isolation was obtained as a byproduct of conventional clinical plasmapheresis through the cooperation of the North Carolina Memorial Hospital Blood Bank. In some cases, outdated human plasma was obtained from the American Red Cross Center, Durham, NC. Human prothrombin and factor X were purified from 6 to 8 L of fresh frozen plasma by the method of DiScipio et al. (10) with the modifications described by Cutsforth et al. (9). Factor X was stored in a buffer containing 1 mM benzamidine, 0.05 M Tris,¹ pH 7.4, 0.02 M sodium citrate, and 0.25 M NaCl in 1 mL aliquots at -70°C until used. Prothrombin was stored in 1 mL aliquots at -70°C in a buffer composed of 50 mM Tris, pH 7.4, 300 mM NaCl, 1 mM benzamidine, and 1 mM phenylmethanesulfonyl fluoride. One day before an experiment, prothrombin was repurified by HPLC on a Series 200 Isopure LC system (Perkin-Elmer Corp., Norwalk, CN) using a Mono Q HR 5/5 ion-exchange column (Pharmacia, Norwalk, CN) (23) and dialyzed into either 50 mM Tris, 175 mM NaCl, 5 mM CaCl_2 , 0.6% PEG, pH 7.6, buffer or 50 mM Tris, 100 mM NaCl, 5 mM Ca^{2+} , pH 7.4, buffer.

Factor X_a was obtained from purified factor X (>97% by SDS-PAGE) activated with purified factor X-activating enzyme from Russell's viper venom coupled to Affi-Gel ester agarose beads [Bio-Rad, Richmond, CA (18)]. Factor X_a was assayed with the synthetic substrate S-2765¹ (19) using active site titrated factor X_a for a standard (17).

Human Pre2 and F1.2 were generated from cleavage of prothrombin at Arg²⁷⁴-Thr²⁷⁵ by factor X_a in the presence of the reversible thrombin inhibitor DAPA by a procedure analogous to that used for bovine prothrombin (41). The reaction mixture contained prothrombin (~50 mg), factor X_a (1:10 molar ratio with prothrombin), and DAPA (10:1 molar ratio with prothrombin) in 25 mM Hepes,¹ 150 mM NaCl, 5 mM Ca^{2+} , pH 7.0, buffer. Pre2 was further purified by HPLC on a Perkin-Elmer Isopure HPLC system (Norwalk, CT) using a Mono Q HR 5/5 ion-exchange column (Pharmacia, Piscataway, NJ) and stored at -70°C in the presence of 1 mM benzamidine and 1 mM phenylmethanesulfonyl fluoride. F1.2 was also purified by HPLC on a Perkin-Elmer Isopure HPLC system (Norwalk, CT) using a Mono Q HR 5/5 ion-exchange column (Pharmacia, Piscataway, NJ) and stored at -70°C in the presence of 1 mM benzamidine and 1 mM phenylmethanesulfonyl fluoride.

Human MzII_a was generated with ECV linked to Affi-Gel active ester agarose (Bio-Rad, Richmond, CA) at a final activity of 2.5 mg of ECV/mL of wet, packed gel. Human prothrombin (3 mL at ~10 μM final concentration) was incubated in a 4 mL fluorescence cuvette with 300 μL of ECV-linked gel in the presence of DAPA (5:1 molar ratio to prothrombin), 5 mM CaCl_2 , 50 mM Tris, and 100 mM NaCl, pH 7.73 at room temperature. The reaction was monitored by the increase in fluorescence resulting from the DAPA-MzII_a complex. Once the reaction was complete, the ECV-linked gel was removed by low-speed centrifugation, and the MzII_a was filtered through a 0.2 μm nonpyrogenic filter (Costar, Cambridge, MA), flash frozen, and

stored in 1 mL aliquots at -70°C . The extent of prothrombin conversion to MzII_a was determined by SDS-PAGE¹ under both nonreducing and reducing conditions and was always >95%.

Protein concentration was estimated from the absorbance at 280 nm after correction for light scattering measured at 320 nm, assuming that scattering scaled as the fourth power of the wavelength. The concentrations of human prothrombin and MzII_a were determined using a molecular weight of 72000 and an extinction coefficient of 1.47 mL $\text{mg}^{-1}\text{cm}^{-1}$ (24). Other values for extinction coefficients were 1.92 mL $\text{mg}^{-1}\text{cm}^{-1}$ for prothrombin 1 (MW 50000) and MzII_a-des fragment 1, 1.73 mL $\text{mg}^{-1}\text{cm}^{-1}$ for Pre2 (MW 37000), and 1.23 mL $\text{mg}^{-1}\text{cm}^{-1}$ for fragment 1.2 (MW 34500) (4).

Phospholipid Vesicles. Extruded large unilamellar vesicles (LUV)¹ composed of 25:75 bovine PS and POPC were prepared by the procedure of Mayer et al. (27) in a buffer containing 20 mM TES and 150 mM NaCl at pH 7.5. Phospholipid concentrations were determined by an inorganic phosphate assay (6).

Kinetic Experiments. (1) Pre2 Formation. SDS-PAGE on a 10% T, 3.5% C resolving gel and a 3.125% T, 20% C stacking gel (8) was performed using a Bio-Rad 130A electrophoresis cell (Bio-Rad, Richmond, CA) to detect proteolysis fragments of prothrombin (Pre2, MzII_a, and II_a) (46). Detection was accomplished either by using [¹²⁵I]-prothrombin for experiments performed in the absence of membranes or by using colloidal Coomassie Blue (28) for experiments performed with unlabeled prothrombin in the presence of membranes (20, 50, 200, and 2000 μM). Aliquots were removed from the reaction mixture and added to a low ionic strength buffer (8 mM Tris, pH 8.3, containing 0.002 M Na_2EDTA and 1% SDS) to arrest the reaction. Both reducing and nonreducing gels were run for each time point along with standards. Iodination of prothrombin (1–8 mg batches) was accomplished by published methods (26). For radiographic detection, gels were dried on a Hoeffer SE 540 gel dryer (Hoeffer Scientific, San Francisco, CA) between porous cellophane sheets (Hoeffer, SE 542). Quantitation was accomplished by exposing Min-R medical X-ray film (Eastman Kodak, Rochester, NY) to the dried gels in a Kodak X-Omatic cassette without intensifying screens (42). Autoradiographs as well as Coomassie-stained gels were scanned with either a Hoeffer GS-300 or LKB UltroScan XL densitometer for experiments performed in the absence of membranes or using a HP Scanjet 6350 C scanner coupled with a software (UNSCAN ITGEL package, version 5.1, Silk Scientific Corp., Orem, UT) to digitize the Coomassie-stained gel run in the presence of membranes. In addition to the proteolysis samples, each gel contained several dilutions of [¹²⁵I]prothrombin or prothrombin used to construct standard curves that related measured densities to the concentration of prothrombin. These standard curves, calibrated to synthetic substrate assays, were used to determine concentrations for the various peptide species in the proteolysis mixture. The rate of Pre2 formation was estimated in the absence of membranes using SDS-PAGE, because the consumption of Pre2 was slower than its rate of production under this condition. However, this method could not be used to estimate the rate of Pre2 formation in the presence of membranes, since, under these conditions, the rate of Pre2 consumption was likely comparable to the rate

of formation. Nonetheless, the time courses of Pre2, MzII_a, and II_a appearance on SDS–PAGE were used to estimate the first-order rate constant for release of Pre2 and MzII_a available to be Michaelis–Menten substrates for the second step of the parallel-sequential activation pathway, as described in Appendix A.

(2) *MzII_a and MzII_a Plus Thrombin Appearance.* The determination of initial rates of MzII_a and II_a plus MzII_a appearance was carried out as described by Rosing et al. (37) using the synthetic substrate S-2238. Prothrombin activating mixtures contained prothrombin and factor X_a in 50 mM Tris, 175 mM NaCl, 5 mM Ca²⁺, and 0.6% PEG,¹ pH 7.6 at 37 °C. Aliquots from the reaction mixture were quenched at different times with soybean trypsin inhibitor (0.33 mg/mL; final concentration in the sample). Small (5 μL) samples from each aliquot (containing 10–100 nM active site) were added to the sample wells of a 96-well Falcon 3912 Microtest III flexible assay plate (Becton Dickinson, Oxnard, CA). Each well contained 105 μL of buffer (38 mM Tris, 170 mM NaCl, 0.6% PEG, pH 7.9) equilibrated at 37 °C on a SLT 340 ATTC microplate reader (SLT Labinstrument, Hillsborough, NC). S-2238 stock solution (35 μL of 0.47 mg/mL with 20 mM Ca²⁺) was added to the well, and the mixture was allowed to equilibrate for 4 s at 37 °C with shaking. Then, the absorbance at 405 nm was recorded for 1 min so as to obtain the initial rate of S-2238 hydrolysis from the linear rate of absorbance change. The concentration of active site (II_a¹ plus MzII_a) exposed at each time point was found by comparing the initial rate of S-2238 hydrolysis to a standard curve that had been prepared using active site titrated thrombin (5). To measure the amount of MzII_a formed, the amidolytic activity was also measured after incubation of the reaction mixture aliquot for 1 min in the presence of heparin (10 μg/mL) and antithrombin III (300 nM) to block the thrombin but not MzII_a active site (38). The rate of MzII_a appearance in the presence of membranes could not be taken to define the rate of MzII_a formation, since this intermediate was consumed at a rate comparable to that at which it was formed. As for Pre2, the first-order rate at which MzII_a became available as a Michaelis–Menten substrate for the second step of activation was estimated as described in Appendix A.

(3) *Pre2 and MzII_a Activation.* The formation of thrombin from Pre2 and MzII_a as substrates was monitored at 37 °C by recording the change in the fluorescence intensity of DAPA¹ bound to exposed active sites, using an SLM 48000MHF spectrofluorometer (SLM Instruments, Inc., Rochester, NY). The excitation wavelength was 280 nm, the emission wavelength was 540 nm, and a 515 cutoff filter was used in the emission path. Since excitation is at the Trp absorption peak, excited-state energy in this assay is transferred from protein to bound DAPA, resulting in enhanced sensitivity relative to that obtained when exciting at the absorption band of DAPA. Pre2 (0.5–2 μM) or MzII_a (2–9 μM) and factor X_a (1.5 or 0.19 μM) in buffer (50 mM Tris, 100 mM NaCl, 5 mM CaCl₂, pH 7.4) containing DAPA¹ (2:1 or 5:1 molar ratio to Pre2 or MzII_a, respectively) were continuously stirred in a microcuvette (Hellma Cells, Inc., Forest Hills, NY) at a volume of 0.8 mL (10 mm path length). Buffers were filtered through 0.2 μm Nalgene filters (Nalge Co., Rochester, NY) to reduce scattering artifacts. The initial rate of thrombin generation was determined at

37 °C from the initial rate of fluorescence intensity change normalized to the intensity at complete thrombin formation (30). The fluorescence intensity at complete thrombin formation was obtained by adding 20 μL of ECV solution (1 mg/mL) to convert all intermediate to thrombin. Fluorescence scans recorded for DAPA and MzII_a in the absence of factor X_a corrected for MzII_a autolysis (33).

(4) *Prothrombin Proteolysis Kinetics Detected by DAPA Fluorescence.* DAPA was also used to monitor continuously the progress of prothrombin activation. Fluorescence intensity was monitored as described for Pre2 and MzII_a activation. Experiments presented here contained DAPA in a molar ratio of 2:1 with prothrombin. Prothrombin (at concentrations of 0.5–2 μM) was incubated with the reaction buffer in the cuvette for 6 min. An appropriate amount of LUV suspension was added in order to reach the desired lipid concentration. The fluorescence at this point was corrected for light scattering (only significant at 2 mM lipid) to obtain the initial DAPA fluorescence [*F*(0)]. An appropriate amount of factor X_a was added (*t* = 0), and the time course of activation was then recorded continuously by monitoring fluorescence intensity. The fluorescence at the end point of activation was determined by adding 10 μL of a Taipan snake venom stock (12.5 mg/mL) to convert all prothrombin to thrombin. DAPA forms a complex not only with thrombin (31) but also with the intermediates in the prothrombin activation pathway, Pre2 and MzII_a (14, 22). Thus, if the relative fluorescence efficiencies of the DAPA complexes with these proteins are known, the time course of DAPA fluorescence contains, in principle, information about both the rate and pathway of prothrombin activation (22). For this reason, DAPA fluorescence time courses were compared with time courses of active site formation and Pre2 formation as an internal test of the accuracy of these more difficultly measured time courses (see Appendix B for a description of how this was accomplished).

RESULTS

Prothrombin Proteolysis by Factor X_a in the Absence of Membranes. Carlisle and Jackson showed that activation of bovine prothrombin 1 in the absence of membranes and factor V_a could be described by the parallel-sequential model and involved both the MzII_a-des fragment 1 and Pre2 intermediates (4). MzII_a-des fragment 1 was very recently confirmed as an intermediate during human prothrombin 1 activation (1). While Carlisle and Jackson were able to estimate rate constants for all four steps of the parallel-sequential pathway as applied to bovine prothrombin 1 activation, these data do not exist for activation of human prothrombin and are essential to the analysis of the role of PS-containing membranes that we have undertaken.

(A) *MzII_a and Pre2 Proteolysis to Thrombin.* Under our conditions, the fluorescence yield of DAPA bound to MzII_a is roughly 25% greater than that of DAPA bound to thrombin (Table 2), resulting in a drop in fluorescence intensity as MzII_a is converted to thrombin by factor X_a (32). The initial slope of this curve, relative to the fluorescence at completion of the reaction, can be related (after correcting for the rate of MzII_a autolysis) to the initial rate of MzII_a conversion to thrombin. This initial rate was a linear function of MzII_a concentration from 2 to 9.5 μM with a slope yielding an apparent second-order rate constant of 14600 M⁻¹ s⁻¹, as recorded in Table 1.

Table 1: Rate Constants^a for Proteolysis of Prothrombin and Its Fragments

reaction/ conditions	variable [X _a], no PL (soln)	5 nM X _a , 20 μM PL	5 nM X _a , 50 μM PL	5 nM X _a , 200 μM PL	5 nM X _a , 2 mM PL
A/Pre2 formation	$(1.10 \pm 0.04) \times 10^3$ ^c $K_M > 100^c$ [1.4×10^3] ^b	$(2.10 \pm 0.01) \times 10^3$	$\leq 6 \times 10^2$ ^c	$\leq 6 \times 10^2$ ^c	$(5.7 \pm 1) \times 10^2$ ^c
B/Pre2 activation	86 ± 7 [113] ^b	$(1.5 \pm 0.2) \times 10^5$	$(1.1 \pm 0.1) \times 10^5$	$(1.3 \pm 0.2) \times 10^5$	<200
C/MzII _a formation	44 ± 10^d [98] ^b	$(8.9 \pm 0.5) \times 10^3$ $k_{cat} = (1.15 \pm 0.3) \times 10^{-2}$ ^g $K_M = 1.3 \pm 0.4$ ^e	$(3.3 \pm 0.3) \times 10^4$ $k_{cat} = (4.7 \pm 0.9) \times 10^{-2}$ ^g $K_M = 1.4 \pm 0.4$ ^e	$(1.47 \pm 0.01) \times 10^4$ $k_{cat} = (3.2 \pm 0.9) \times 10^{-2}$ ^g $K_M = 2.2 \pm 0.6$ ^e	$(4.5 \pm 0.1) \times 10^3$
D/MzII _a activation	$(1.46 \pm 0.14) \times 10^4$ $K_M > 20$ [1.5×10^4] ^b	$(3.7 \pm 0.7) \times 10^{6f}$ $k_{cat} = 2.8 \pm 0.3$ $K_M = 0.76 \pm 0.23$	$(1.6 \pm 0.1) \times 10^{6f}$ $k_{cat} = 1.35 \pm 0.08$ $K_M = 0.85 \pm 0.13$	$(2.79 \pm 0.04) \times 10^{6f}$ $k_{cat} = 5.3 \pm 0.1$ $K_M = 1.9 \pm 0.06$	$(0.54 \pm 0.04) \times 10^6$
E/channeling	0	$(1.5 \pm 0.3) \times 10^3$ ^h $k_{cat} = (1.9 \pm 1) \times 10^{-3}$	$(3.9 \pm 0.4) \times 10^4$ ^h $k_{cat} = (5 \pm 1) \times 10^{-2}$	$(1.44 \pm 0.02) \times 10^4$ ^h $k_{cat} = (3.2 \pm 0.8) \times 10^{-2}$	0
channeling ⁱ f	0	0.12	0.51	0.47	0

^a Second-order rate constants (k_{cat}/K_M) have units of (M product) (M substrate)⁻¹ (M bound X_a)⁻¹ s⁻¹ = M⁻¹ s⁻¹. When available, apparent Michaelis–Menten constants are also given with units of s⁻¹ (k_{cat}) or μM (K_M). Error estimates derive from uncertainties in hyperbolic parameters (k_{cat} and K_M) or of slopes (k_{cat}/K_M) of initial rates versus substrate concentration. All rate constants obtained by the regression analysis described in Appendix A are italicized. ^b Values for proteolysis of bovine prothrombin 1 by bovine factor X_a reproduced from Carlisle et al. (4) for reference. ^c Since no Pre2 could be detected in SDS–PAGE experiments, this upper limit is based on the limit of detection of our gels. ^d This parameter was estimated by minimizing manually the sum of squared residuals of calculated and observed MzII_a and II_a concentration versus time (Figure 2A). An estimate of the uncertainty was obtained as the largest change in the parameter resulting in a doubling of the sum of squared residuals. ^e K_M values are from hyperbolic fits of the rate of MzII_a appearance versus MzII_a concentration (Figure 5A), with the errors being the standard parameter errors obtained from the fitting. ^f k_d used for regression of the parallel-sequential or three-pathway models was obtained from k_{cat}/K_M and the K_M for reaction C, as described in Results. ^g k_{cat} for reaction C was obtained from estimates of the first-order rate constants (k_c) obtained by least squares regression using the expression $k_{cat} = (k_c/[X_a]_{bound})/([II]_0 + K_M^C)$. Uncertainties in k_c (standard parameter errors from SigmaPlot) and K_M^C (see footnote e) were translated to uncertainties in k_{cat} as $dk_{cat} = dk_c/[X_a]_{bound}([II]_0 + K_M^C) + k_c/[X_a]_{bound} dK_M^C$. ^h First-order rate constants for direct conversion of prothrombin to thrombin (reaction E in Figure 1) were obtained by least squares regression analysis (Appendix A). These were converted to k_{cat} values as described in footnote g, using K_M values for reaction C. ⁱ The fraction of prothrombin channeled to thrombin via either the MzII_a or Pre2–F1.2 intermediates was calculated as $f = k_c/(k_a + k_c + k_e)$.

Since the fluorescence of DAPA bound to thrombin is roughly 10 times greater than for DAPA bound to Pre2 (Table 2), proteolysis of Pre2 leads to an increase in fluorescence intensity. However, the rate of Pre2 proteolysis was so slow that no reaction could be detected unless the concentration of factor X_a was high. A very slow increase in DAPA fluorescence could be detected for conversion of Pre2 to thrombin by 1.53 μM factor X_a. Addition of ECV calibrated the fluorescence signal for 100% conversion to thrombin. The rate of thrombin generation was linear with Pre2 concentration up to 2 μM, yielding an apparent second-order rate constant of 86 M⁻¹ s⁻¹, as recorded in Table 1. Experiments performed with F1.2 present at the same concentration as Pre2 gave the same rate.

(B) *Kinetics of Prothrombin Proteolysis to Pre2.* Activation of [¹²⁵I]prothrombin by factor X_a in the absence of phospholipid and factor V_a was followed by SDS–PAGE at high enzyme concentration (0.75 μM) due to the slow rate of reaction. Pre2 was the major activation product detected at early times (up to 12–15 min). After 15–20 min, the Pre2 band started to spread toward lower molecular weights. This band shift was not observed in the presence of the thrombin inhibitor DAPA.¹ We interpret this as due to conversion of Pre2 to des-(1–13) Pre2 through the action of thrombin or MzII_a, which must then be present in the activation mixture even at early times. Thrombin and MzII_a degrade Pre2 because human prothrombin contains an Arg²⁸⁶–Thr²⁸⁷ bond, which is susceptible to cleavage by thrombin (11). By 90 min (as long as the reaction was followed), the Pre2 band was roughly equally distributed between the whole and des-(1–13) forms. At these long reaction times, thrombin heavy chain was clearly seen below the Pre2 band. For analysis of the kinetics of Pre2 formation, the total amount of product was taken to be the integrated area in the Pre2

Table 2: Characteristics of DAPA–Protein Complexes

protein (<i>i</i>)	K_d	q_i/q_{0d}
thrombin (1)	2.0×10^{-8} 2.0×10^{-8} (14) 4.3×10^{-8} (31) 1.7×10^{-8} (33)	32.4 ± 0.1 (3) ^a
MzII _a (2)	5.9×10^{-8} 5.9×10^{-8} (33)	40.2 ± 0.2 (3) ^b
Pre2 (3)	5.9×10^{-8} (22) 4.5×10^{-7} 5.9×10^{-7} (14)	3.7 ± 0.1 (2) ^a

^a Number of determinations. ^b Three determinations at different [MzII_a] led to an extrapolated value as [MzII_a] → 0. The error was estimated from the uncertainty in the extrapolation.

and des-(1–13) Pre2 bands. The results of one such experiment are plotted in Figure 2A as open triangles.

Several experiments were performed at different prothrombin concentrations (3–50 μM) in which the conversion of prothrombin to Pre2 was followed by SDS–PAGE. Apparent K_M and k_{cat} values could not be obtained from the resulting time courses via the integrated Michaelis–Menten equation, presumably because the apparent K_M for this reaction is larger than the substrate concentrations used. From six such experiments, we obtained an average apparent second-order rate constant of 1067 ± 300 s⁻¹ M⁻¹. In a subsequent classical Michaelis–Menten experiment, special effort was made to cover a large range of prothrombin concentrations (4–75 μM). Even with data going to this high substrate concentration, there was insufficient curvature in a plot of initial rate versus substrate concentration to yield a meaningful estimate of the K_M . The estimate obtained for k_{cat}/K_M (1040 ± 40 s⁻¹ M⁻¹) from these measurements agreed well with the apparent second-order rate constant obtained from our first series of experiments using the

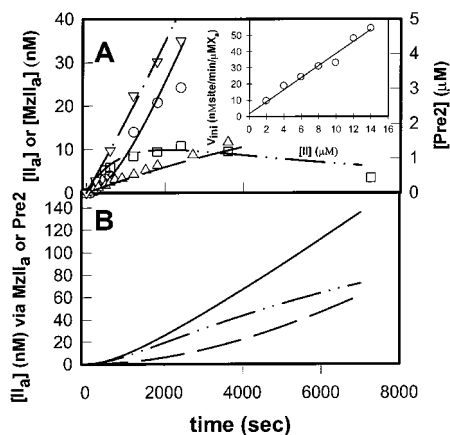


FIGURE 2: Time course of MzII_a or MzII_a plus thrombin appearance. (A) A reaction mixture containing prothrombin (4 μM), factor X_a (91 nM), 50 mM Tris (pH 7.6), 175 mM NaCl, 5 mM Ca²⁺, and PEG (0.6%) at 37 °C was monitored by the rate of S-2238 hydrolysis in the presence (MzII_a only, squares) and absence (MzII_a plus thrombin, inverted triangles) of heparin (10 μg/mL) and antithrombin III (300 nM). The difference between these two observations gives the time course for the production of thrombin (circles). The appearance of Pre2 (triangles; note scale on right ordinate) was measured using SDS–PAGE. The lines represent the simulated time course for the appearance of thrombin (solid), MzII_a (dot-dot-dashed), thrombin and MzII_a (dot-dash), and Pre2 (dashed) using the parallel-sequential model and the kinetic parameters measured in this work (Table 1). The insert shows the initial rate of total active site (open circles) appearance as a function of prothrombin concentration, with the straight line through these points defining the apparent k_{cat}/K_M of $62 \pm 4 \text{ M}^{-1} \text{ s}^{-1}$. (B) A simulation of prothrombin proteolysis by the parallel-sequential mechanism is shown in terms of total thrombin (solid line) and the amounts of thrombin that appear via the MzII_a (dot-dot-dashed line) and Pre2 (dashed line) intermediates.

integrated Michaelis–Menten method and is reported in Table 1. From these data, we conclude that $K_M > 200 \mu\text{M}$ and $k_{cat} > 0.2 \text{ s}^{-1}$.

(C) *MzII_a and Thrombin Appearance.* Figure 2A also shows the time course for the appearance of total active site concentration (inverted triangles) observed using the synthetic substrate S-2238 for 4 μM prothrombin. The overall initial rate of total active site formation was linear in prothrombin concentration up to 15 μM (insert to Figure 2A) and yielded an apparent k_{cat}/K_M of $62 \pm 4 \text{ M}^{-1} \text{ s}^{-1}$, with $K_M > 25 \mu\text{M}$. Upon incubation for 1 min in the presence of antithrombin III plus heparin, the thrombin active site is blocked, and only MzII_a is detected (38). Both these data (squares in Figure 2A) and the large rate of MzII_a proteolysis (Table 1) make it clear that MzII_a appears transiently during the activation of prothrombin by factor X_a in solution. This made it impossible to estimate the rate of prothrombin proteolysis to MzII_a (reaction C of Figure 1) directly from the rate of MzII_a appearance. This could reflect slow formation of MzII_a coupled with its rapid conversion to thrombin. To obtain the time course of thrombin generation, the time course of MzII_a appearance was subtracted from the time course of total active site appearance, with the result being plotted as circles in Figure 2A. The appearance of Pre2 was followed via SDS–PAGE and is shown as triangles in Figure 2A. In the early stages of proteolysis, the appearance of active sites was, as expected, due mainly to formation of MzII_a.

(D) *Simulation of Prothrombin Activation and Kinetics of MzII_a Formation.* Table 1 summarizes the rate constants

obtained here for the factor X_a-catalyzed proteolysis of human prothrombin (reaction A, Figure 1), Pre2 and F1.2 (reaction B), and MzII_a (reaction D). The second-order rate constant for MzII_a formation ($44 \pm 10 \text{ M}^{-1} \text{ s}^{-1}$; reaction C) was obtained by fitting the time courses in Figure 2A to the parallel-sequential reaction mechanism (eqs A1–A4). The solid lines in Figure 2A demonstrate that the observed rate of thrombin formation and Pre2 and MzII_a appearance could be predicted quite well by the parallel-sequential model. The predicted thrombin appearance curve shows clearly the lag phase and the MzII_a curve the maximum expected for a two-step, sequential mechanism. These features are also evident in the experimental data (circles for thrombin; squares for MzII_a).

Our simulation procedures (Appendix A) show that, under the conditions of the experiment shown in Figure 2A, the initial thrombin formed by the action of factor X_a derived almost exclusively from the MzII_a intermediate (Figure 2B, dot-dot-dashed curve), while the Pre2 intermediate contributed to thrombin formation only at long reaction times (Figure 2B, dashed curve).

Our conclusions regarding the mechanism of human prothrombin activation in the absence of lipid and factor V_a agree entirely with those reached by Carlisle et al. (4) for activation of bovine prothrombin 1 (prothrombin missing its membrane binding, N-terminal piece, fragment 1; see Figure 1). Indeed, the apparent second-order rate constants obtained here are also in general agreement with those reported by Carlisle et al. for the bovine proteins (see Table 1). These results are useful in two ways. First, they establish the similar functionality of the bovine and human forms of factor X_a and prothrombin in the absence of membranes and factor V_a. This agreement is expected from (1) similarities in the second-order rate constants for activation of the human and bovine forms of MzII_a and Pre2 by the full prothrombinase complex (21, 30), (2) similarities in the binding affinities of the human and bovine forms of prothrombin and factor X_a to acidic lipid membranes (9), and (3) similarities in conformational changes in bovine and human prothrombin associated with membrane binding (45). Second, the expected agreement of our results with those of Carlisle et al. serves to validate our method for estimating the kinetic constants for activation of human prothrombin by factor X_a.

Prothrombin Proteolysis by Factor X_a in the Presence of Membranes. (A) *Time Courses of MzII_a and Thrombin Appearance.* The thrombin-specific chromogenic substrate S-2238 is hydrolyzed equally well by the active site of MzII_a or thrombin and thus can detect the presence of both, as described in Methods. Initial time courses for activation of 1 μM prothrombin to MzII_a and thrombin by 5 nM factor X_a in the presence of Ca²⁺ and different concentrations of PS/POPC (25:75) LUV are shown in Figure 3. Panel A shows that the time course of MzII_a appearance was linear for all lipid concentrations over the time range investigated. From panel B of this figure, it is evident that the same is not true of the time course of thrombin formation, which showed a lag phase at very low (20 μM, squares) or very high (2 mM, triangles) lipid concentrations. This implies the existence of a sequential reaction pathway at these two lipid concentrations, with the accumulation of one or more intermediates that are then converted to thrombin. The

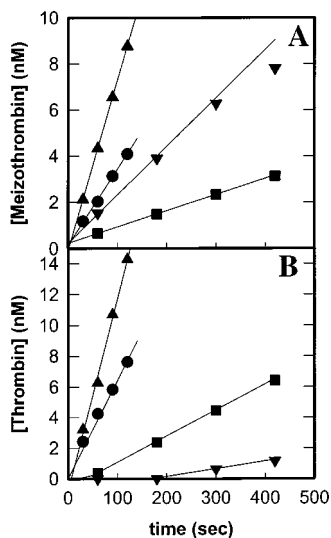


FIGURE 3: Initial time courses of meizothrombin and thrombin formation. (A) The appearance of MzII_a with time of incubation (abscissa) at 37 °C was monitored by the rate of S-2238 hydrolysis in the presence of heparin (10 µg/mL) and ATIII (300 nM). (B) The appearance of MzII_a plus thrombin with time of incubation (abscissa) at 37 °C was monitored by the rate of S-2238 hydrolysis in the absence of heparin (10 µg/mL) and ATIII (300 nM). Thrombin formation was determined as the difference between the contribution of the active site detected by S-2238 hydrolysis in the absence and presence of heparin and ATIII (see Methods). The reaction mixture contained 1 µM prothrombin, 5 nM factor X_a, 50 mM Tris (pH 7.6), 175 mM NaCl, 5 mM Ca²⁺, 0.6% PEG, and different concentrations of PS/POPC (25:75) LUVs: 20 µM (filled squares); 50 µM (filled triangles); 200 µM (filled circles); 2 mM (filled inverted triangles). Straight lines were obtained using least squares linear regression on all points except the zero time point.

intermediate could be either MzII_a or Pre2 and F1.2. The essentially linear reaction time courses seen at intermediate lipid concentrations are not necessarily inconsistent with a sequential, two-step reaction mechanism, but if this mechanism obtains, these time courses do imply that intermediate is converted to thrombin very rapidly once it is formed.

It is also worth noting about the time courses in Figure 3 that the initial rates of MzII_a or thrombin formation did not increase with lipid concentration in a simple monotonic fashion. To reveal more clearly the lipid dependence of prothrombin activation by factor X_a, we have plotted in Figure 4A the initial rate of MzII_a and thrombin formation as a function of lipid concentration at a single prothrombin concentration (0.5 µM). Several features of these data deserve comment. First, the rate of thrombin formation (open circles) increased dramatically from 0 to 50 µM phospholipid and then also decreased rather quickly up to 200 µM. Above 200 µM lipid, the rate of thrombin formation continued to decrease, but much less dramatically. Second, the rate of MzII_a appearance showed a less dramatic optimum than seen for thrombin formation at 50 µM lipid and was roughly constant from 50 to 200 µM lipid. In the range of lipid concentration from 50 to 200 µM, the rate of thrombin formation was greater than the rate of MzII_a appearance (Figure 4A). This might mean that significant thrombin formed through the Pre2 pathway under these conditions or that most MzII_a produced was very rapidly processed to thrombin and thus not detected. It was in this intermediate lipid concentration range that thrombin formation was linear

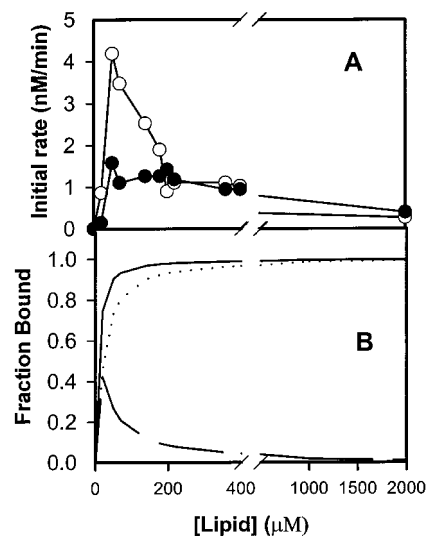


FIGURE 4: Initial rates of prothrombin activation as a function of phospholipid (PS/POPC, 25:75, LUV) concentration. Active site development at 37 °C (thrombin and MzII_a or MzII_a formation; see Methods) was determined by S-2238 assays. Reaction mixtures contained 0.5 µM prothrombin, 5 nM X_a, 50 mM Tris (pH 7.6), 175 mM NaCl, 5 mM CaCl₂, and 0.6% PEG. The concentration of PS/POPC (25:75) membranes was varied from 0 to 2000 µM. Panel A records the initial rate of MzII_a formation (filled circles) and thrombin formation (open circles) as a function of phospholipid concentration. Panel B shows the calculated fraction of factor X_a bound to lipid (solid line), the fraction of prothrombin bound to lipid (dotted line), and the fraction of lipid surface occupied by bound protein (dashed line). The calculations and binding constants used are documented in Powers and Lentz (34).

with time (Figure 3B). The implication of these observations is that, for this intermediate lipid concentration, any intermediate formed (MzII_a or Pre2) must be very rapidly converted to thrombin.

(B) *Apparent Michaelis–Menten Parameters for MzII_a and Thrombin Formation.* For two reasons, the steady-state kinetic constants for prothrombin activation by factor X_a in the presence of membranes were more difficult to determine than by factor X_a alone in solution. First, the concentration of the enzymatic species of interest (factor X_a bound to the surface) is a function not only of lipid but also of substrate concentration. In general, competition between the substrate and enzyme for the membrane was minimal except under conditions of very high substrate concentration and low lipid concentration, but the linkage between these binding equilibria still had to be taken into account using methods described previously (34). Figure 4B shows the fractions of factor X_a (solid line) and of prothrombin (dotted line) bound to membrane at each lipid concentration under the conditions of the experiments recorded in Figure 4A. Note that the peak in the rate of thrombin formation corresponded to saturation of factor X_a binding even though only about 75% of prothrombin was bound at this lipid concentration. Also shown as a dashed line is the fraction of membrane surface occupied by bound proteins. This was maximal at 20 µM lipid, a concentration for which prothrombin binding was well below saturation and at which the rates of MzII_a and thrombin formation were still suboptimal. These curves suggest that the maximum rate of thrombin generation occurred at a lipid concentration for which there was a balance between the extent of prothrombin binding and the

density at which factor X_a and prothrombin occupied the membrane surface.

Second, competition for the substrate exists between membrane-bound factor X_a and factor X_a free in solution. For most cases, the contribution to prothrombin activation from solution factor X_a was insignificant, but one must still account for the fraction of total factor X_a that is bound to the membrane in analyzing kinetic experiments. There is also the question of whether to consider only membrane-bound substrate. In all cases, initial rates were expressed *per bound factor X_a concentration*, and the *total substrate concentration*² was used to obtain k_{cat} and K_M kinetic constants for the membrane-bound enzyme. In every instance, initial rates are presented in terms of “product formed per unit time per membrane-bound factor X_a ”.

For several key lipid concentrations, the procedures described above were used to obtain the initial rate of thrombin formation or MzII_a appearance as a function of substrate concentration (Figure 5). Except at the highest lipid concentration (2 mM, inverted triangles), the initial rate of MzII_a appearance (Figure 5A) showed saturable behavior with substrate concentration, typical of a normal Michaelis–Menten description. From these curves were obtained the *apparent steady-state k_{cat} and K_M values*. The k_{cat} values (0.13 ± 0.06 , 2.5 ± 1.1 , and 1.1 ± 0.4 s⁻¹ for 20, 50, and 200 μ M membranes, respectively) peaked at 50 μ M membranes, while K_M (Table 1) showed little variation in the range from 20 to 200 μ M membranes. At 2 mM PS/POPC membranes, only k_{cat}/K_M could be defined [$(0.38 \pm 0.03) \times 10^4$ M⁻¹ s⁻¹], implying that $K_M > 5$ μ M. As seen from the table, the rates obtained in the presence of membranes were much larger than those observed in the absence of membranes. Note that, because MzII_a is consumed as it is formed, *these apparent rate constants for MzII_a appearance are lower limits to the actual rates of MzII_a formation*.

The Michaelis–Menten plots for thrombin formation were much more complex, as shown in Figure 5B. At a very high lipid concentration (2 mM, inverted triangles), a linear increase in rate with prothrombin concentration was seen, and a seemingly normal saturable behavior was seen at 200 μ M lipid (circles). However, the initial rate of thrombin formation at low and intermediate lipid concentrations (20 μ M, squares; 50 μ M, triangles) showed first a saturable behavior and then a secondary increase with increasing prothrombin concentrations (Figure 5B, squares and inverted triangles, respectively). We estimated the second-order rate constant [$(3.4 \pm 0.3) \times 10^4$ M⁻¹ s⁻¹] for the overall activation of prothrombin to thrombin at 50 μ M PS/POPC membranes from a linear fit to the initial part of the inverted triangle data in Figure 5B. Using our methods for estimating concentrations of prothrombinase species (34), we calculated that the fraction of prothrombin that was membrane bound varied with the concentration of prothrombin in a reaction mixture at these low lipid concentrations. At low substrate concentrations, most of the substrate and factor X_a are bound

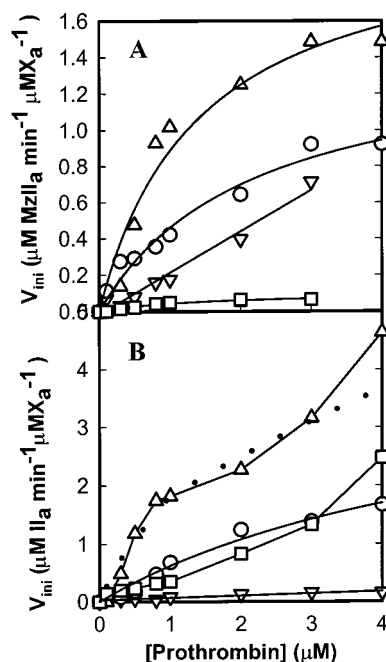


FIGURE 5: Meizothrombin and thrombin formation as a function of prothrombin concentration. The initial rate of MzII_a (A) or II_a formation (B) (obtained as in Figure 4) is plotted as a function of prothrombin concentration. Prothrombin at a series of concentrations in a total volume of 250 μ L was activated with factor X_a (5 nM) in a buffer containing 50 mM Tris, 100 mM NaCl, and 5 mM CaCl₂ at pH 7.4 and 37 °C with lipid concentrations of 20 μ M (squares), 50 μ M (triangles), 200 μ M (circles), and 2 mM (inverted triangles). Initial rates obtained from the earliest time points of progress curves were corrected by dividing by the fraction of factor X_a bound to membranes. Thus, apparent kinetic constants obtained from hyperbolic fits to these data reflect the activity of membrane-bound factor X_a . Apparent K_M values for MzII_a appearance are recorded in Table 1; these are assumed to characterize MzII_a formation. The apparent k_{cat} values for MzII_a appearance obtained from the fits shown were $(1.7 \pm 0.2) \times 10^{-3}$, $(35 \pm 5) \times 10^{-3}$, and $(24 \pm 3) \times 10^{-3}$ s⁻¹ for 20, 50, and 200 μ M lipid, respectively. For 2 mM lipid, k_{cat}/K_M was $(0.38 \pm 0.03) \times 10^3$ M⁻¹ s⁻¹. Because MzII_a is consumed as it is formed, these values are lower limits to the actual rates at which the MzII_a intermediate is formed and released from the membrane–enzyme complex. For the sake of comparison with the literature, Michaelis–Menten parameters were obtained from fitting the thrombin data by a hyperbola up to the highest prothrombin concentration that would reasonably allow such a fit. Values of k_{cat} and K_M were $(44 \pm 18) \times 10^{-3}$ s⁻¹ and 1.9 ± 1.3 μ M and $(67 \pm 0.002) \times 10^{-3}$ s⁻¹ and 5.5 ± 0.01 μ M for 50 and 200 μ M lipid, respectively, and values of k_{cat}/K_M were $(7.0 \pm 0.4) \times 10^3$ and $(0.64 \pm 0.09) \times 10^3$ M⁻¹ s⁻¹ for 20 μ M and 2 mM lipid, respectively.

to the membrane; but at high substrate concentrations, the membrane becomes crowded. The possible consequences of this crowding will be addressed in the Discussion.

(C) *Kinetics of the Conversion of MzII_a and Pre2 to Thrombin*. DAPA displays different fluorescence properties when complexed with thrombin, Pre2, or MzII_a (14; Table 2). The time course of fluorescence intensity increase thus provides a measure of thrombin generation from Pre2 (in the presence of equimolar amounts of F1.2), as shown in Figure 6A. The first 5–10% of these time courses were nearly perfectly linear, and the initial rate of thrombin formation was obtained by fitting this part of each time course (always <10% completion) to a straight line, as illustrated by the dashed curve in Figure 6A. Plots of the initial rate of thrombin generation were nearly a linear

² We take the position that it is impossible to know at this point whether approach of prothrombin to the factor X_a active site is more effective via the membrane surface or via solution under any particular set of conditions. For this reason, empirical kinetic constants were always calculated in terms of *total prothrombin concentration* and apply only to the membrane and protein concentrations for which they were obtained.

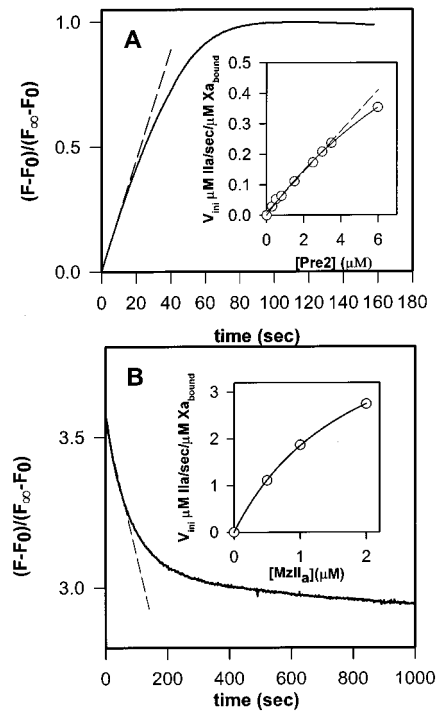


FIGURE 6: Time course of prothrombin 2-fragment 1.2 and MzII_a activation to thrombin. (A) For Pre2 activation, the increase in fluorescence intensity due to formation of the DAPA-thrombin complex was recorded at 37 °C. Plotted is the percent increase of DAPA fluorescence versus time. Percent increase was calculated as the observed fluorescence change ($F - F_0$) due to proteolysis divided by the total fluorescence change ($F_{\text{total}} - F_0$) resulting from activation of Pre2 to thrombin by addition of ECV times 100%. The instrumental setup is described in Methods. The reaction mixture contained 0.3 μM Pre2, 0.6 μM DAPA, 0.3 μM F1.2, 55 nM factor X_a , 75 μM 25:75 PS/POPC LUV, and 5 mM Ca^{2+} in 50 mM Tris and 0.1 M NaCl, pH 7.4. The straight line defining the initial rate was obtained by linear regression of the very early portion of the time course (in this case, 20 s). The insert shows initial rates of thrombin formation as a function of the concentration of Pre2 in the presence of an equal concentration of fragment 1.2. (B) For MzII_a activation, the decrease in fluorescence of DAPA was recorded at 37 °C using an instrumental setup described in Methods. The reaction mixture contained 1.0 μM MzII_a, 5.0 μM DAPA, 5 nM factor X_a , 200 μM 25:75 PS/POPC LUV, and 5 mM CaCl_2 in 50 mM Tris and 100 mM NaCl, pH 7.4. The insert shows a plot of initial rate of thrombin formation as a function of MzII_a concentration.

function of Pre2 concentration up to about 2–3 μM Pre2 (dashed curve in the insert to Figure 6A), which was usually the highest Pre2 concentration considered. The slopes of such lines obtained with 5 nM factor X_a and in the presence of 20 μM , 50 μM , 200 μM , and 2 mM PS/POPC membranes yielded the k_{cat}/K_M values recorded in Table 1. For the experiment carried out at 55 nM X_a and shown in Figure 6A, data were recorded up to 6 μM Pre2, yielding a very slightly curved Michaelis–Menten plot (insert to Figure 6A). This produced a crude estimate of the k_{cat} and K_M of Pre2 activation as $1.2 \pm 0.1 \text{ s}^{-1}$ and $14 \pm 2 \mu\text{M}$, respectively. Since F1.2 binds tightly to Pre2 (29), it is expected that it serves to deliver Pre2 to membrane-bound factor X_a . Not surprisingly, then, the rate of thrombin formation from Pre2 in the absence of F1.2 but in the presence of 75 μM PS/POPC membranes was only $100 \text{ M}^{-1} \text{ s}^{-1}$ (data not shown), essentially indistinguishable from the rate seen in the absence of membranes (Table 1).

Thrombin generation from MzII_a was similarly followed by a change (in this case, decrease) in DAPA fluorescence intensity (Figure 6B). A plot of initial rate versus MzII_a concentration at 200 μM PS/POPC membranes is given in the insert to Figure 6B. For all lipid concentrations studied (20 μM , 50 μM , 200 μM , and 2 mM PS/POPC), the initial rate of thrombin formation was saturable in MzII_a, so all such plots were fit to hyperbola to obtain the k_{cat} and K_M values recorded in Table 1. As for the other proteolysis reactions investigated, the initial rates were expressed at each substrate concentration as rates per concentration of membrane-bound factor X_a so that the resulting steady-state rate constants refer to reactions catalyzed by membrane-bound enzyme only.

(D) *Application of the Parallel-Sequential Model To Estimate Rates of Pre2 and MzII_a Formation.* To obtain rate constants for reactions A and C of the proteolytic scheme shown in Figure 1, we have measured directly the time courses of thrombin and MzII_a (determined by S-2238 and SDS-PAGE) and Pre2 appearance (SDS-PAGE) at lipid concentrations of 20 μM , 50 μM , 200 μM , and 2 mM. These data are presented in the left panels of Figure 7. It is clear that the results from S-2238 activity measurements (open symbols) are in very good agreement with the much more labor-intensive measurements via SDS-PAGE (filled symbols). At 200 μM lipid, we have measured Pre2 appearance at only one time point since no Pre2 was detected at 50 μM and very little was detected at 2000 μM PS/POPC membrane, and a good match was seen between SDS-PAGE and the S-2238 assay at all lipid concentrations. We also calculated fluorescence intensities expected for DAPA-based monitoring of prothrombin proteolysis from the activity-based data shown in Figure 7. This was done using the methods described in Appendix B and the DAPA properties collected in Table 2. The quantitative agreement of these calculated values with actual DAPA fluorescence time courses (not shown) provided a third confirmation of our activity-based time courses. Finally, we attempted to describe the data in Figure 7 in terms of the parallel-sequential model, as described in Appendix A. Since we wished to test the ability of the parallel-sequential model to account for these data, k_c was fixed at 0 (no direct conversion of prothrombin to thrombin) in attempting to describe the data. We kept k_b and k_d fixed at values determined in this paper (Table 1), and k_a and k_c were adjusted to obtain the best possible fit to the three (II_a, MzII_a, Pre2) experimental time courses. Initial estimates of these parameters were the lower limits to k_c obtained from the data in Figure 5A and the value of k_a obtained in the absence of membranes (Table 1).

This procedure makes the inherent assumption that all membrane-bound factor X_a is available for the second steps of the parallel-sequential reaction model, i.e., that $[X_a]_{\text{bound}}$ (membrane-bound X_a) is constant for each step of the reaction mechanism. With this assumption, our initial efforts consistently overestimated the rate of thrombin appearance and underestimated the rate of MzII_a appearance, and only by reducing the value of k_d [rate of MzII_a conversion to thrombin = $(k_{\text{cat}}/K_M)_d[X_a]_{\text{bound}}$] could we reproduce the measured thrombin and MzII_a time courses. We reasoned that not all membrane-bound X_a might be available for the second step of the reaction, since a substantial fraction of X_a might be tied up with the first step of the reaction at the

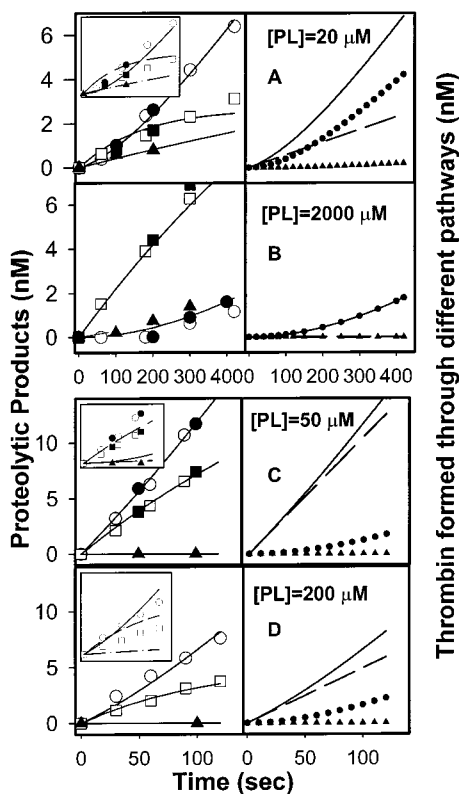


FIGURE 7: Best fits of simulations to observed prothrombin proteolysis data at different lipid concentrations: (A) 20 μM PS/POPC LUVET; (B) 2000 μM PS/POPC LUVET; (C) 50 μM PS/POPC LUVET; (D) 200 μM PS/POPC LUVET. Left panel: Prothrombin (1 μM) proteolysis catalyzed by factor X_a (5 nM) in the presence of PS/POPC (25:75) LUVET (membrane concentrations indicated in right panels) and CaCl_2 (5 mM) was monitored at 37 $^\circ\text{C}$ by thrombin (circles) and MzII_a (squares) activity assays (open symbols) or by SDS-PAGE (closed symbols). The time courses of Pre2 formation detected by SDS-PAGE are presented as filled triangles. Simulated time courses (lines) were calculated according to eqs A1'–A4' using best fit kinetic parameters given in Table 1. For 20, 50, and 200 μM PS/POPC membranes, the inserts show that least squares fits to the thrombin (solid lines), MzII_a (dashed lines), and Pre2 (dot-dashed lines) data were inadequate, and it was necessary to include reaction E of Figure 1 to describe the data adequately (solid lines in the main left-hand frames). Right panel: Simulated quantities of thrombin (solid lines) arising via MzII_a (small squares), Pre2 (small triangles), or channeling (reaction E, dashed lines) are plotted versus time. Simulations were performed using eq A4 and best fit kinetic parameters given in Table 1 and integrating individually up to a desired time the three terms contributing to thrombin formation in this equation.

high prothrombin concentration used in our experiments (1 μM). In other words, prothrombin or product binding to factor X_a might lower $[X_a]_{\text{bound}}$ available for the second step of the reaction ($\text{MzII}_a \rightarrow \text{II}_a$). Rather than introduce an adjustable parameter to account for this substrate competition, we decided to estimate the concentration of membrane-bound factor X_a tied up with the first step of the reaction from the Michaelis–Menten constant (K_M^c) for conversion of prothrombin to MzII_a (reaction C in Figure 1): $[X_a\text{II}]_{\text{bound}} = [X_a]_{\text{bound}}[\text{II}]_0 / (K_M^c + [\text{II}]_0)$, where $[\text{II}]_0$ = initial prothrombin concentration (1 μM) for the reaction conditions used to obtain this table). This gave $k_d = [X_a]_{\text{bound}}(k_{\text{cat}}/K_M)_d \{ K_M^c / (K_M^c + \text{II}_0) \}$, with which we were able to describe our data without introducing any additional parameters. This amounts to

treating K_M^c as an *apparent dissociation constant* for binding of all forms of the substrate (unreacted or cleaved) to membrane-bound X_a in order to estimate the fraction of enzyme available to bind released intermediate for the second step of the reaction.

At high lipid concentration (2 mM), a reasonable description of the data by the parallel-sequential model was possible, and the lines drawn through the data in Figure 7 illustrate the fit obtained. The best fit values of k_a and k_c are given in Table 1. The rate of Pre2 formation (k_a) could be reasonably estimated only at 20 and 2000 μM lipid, where Pre2 was detectable by SDS-PAGE under our reaction conditions. From these regression-adjusted parameters, it is clear that k_a was not altered significantly by the presence of membranes. By contrast, the rate of MzII_a formation (k_c) was increased about 100-fold. The time course for thrombin generation at 2 mM lipid (open squares in Figure 7) shows the positive curvature expected for a sequential process (line in Figure 7) involving accumulation of an intermediate. The appearance of the MzII_a intermediate had a slightly negative curvature over the time interval investigated (circles), as also predicted by the parallel-sequential model (dashed line in Figure 7). The initial rate of thrombin formation was also greater than the sum of the initial rates of Pre2 and MzII_a formation at 2 mM lipid, also consistent with a sequential reaction model. We conclude that the parallel-sequential model was consistent with our data at 2 mM lipid.

The data at 20 μM lipid could be roughly described by the parallel-sequential model but with the appearance of MzII_a somewhat overpredicted and the appearance of II_a somewhat underpredicted (insert to Figure 7).

Under the conditions for which we observed maximal activation rates (intermediate lipid concentrations; see Figure 4A), it was impossible to obtain values for k_a and k_c that would allow a description of all three observed time courses by the parallel-sequential reaction mechanism. This is illustrated for the 50 and 200 μM lipid data by the inserts to the left-hand panels of Figure 7. If the predicted production of thrombin (solid lines in the inserts) approximated the observed (open circles), then the predicted appearance of MzII_a (dashed lines in the inserts) overestimated the observed (open squares), as seen at 200 μM lipid. If the appearance of MzII_a was well matched, thrombin formation was grossly underpredicted (illustrated by the insert for the 50 μM lipid data). Thus, while the parallel-sequential mechanism can account well for factor X_a catalyzed activation of prothrombin in the absence of membranes or at excess or extremely low lipid concentration, it cannot account for observed time courses at optimal lipid concentration. Indeed, the parallel-sequential model could not account for the data *even when the experimentally fixed rates (k_b and k_d) were allowed to vary*. While simulations based on the parallel-sequential model are useful to illustrate this, it is inherently clear that thrombin cannot be produced at a greater rate than are the intermediates (as occurs at 50 μM lipid; see Figure 7) if thrombin must be formed via released intermediates. We conclude that, under these conditions of high surface occupancy of PS/POPC membranes by prothrombin and factor X_a (Figure 4B), the parallel-sequential reaction mechanism is inadequate and a third path for thrombin formation must be considered.

DISCUSSION

A Hypothesis: Intermediate “Channeling” at Optimal Lipid Concentrations. To account for the rapid appearance of thrombin at optimal lipid concentrations, a third pathway was hypothesized (three-pathway model). The rationale for this hypothesis is that, at optimal surface occupancy, intermediate released to the membrane surface should have a finite chance of binding to a membrane-bound factor X_a molecule before it dissociates from the membrane. Effectively, the enzyme and the membrane surface around it should act as an “extended enzyme” with which the intermediate remains associated until a second bond can be cut due to rebinding of the intermediate to the actual membrane-bound factor X_a enzyme. Processing of two or more successive steps of an enzymatic reaction without release of an intermediate is commonly called channeling, and we hypothesized that a membrane surface could act to channel intermediate rapidly to thrombin. The simplest way to model this hypothesis in the context of the parallel-sequential model was to include reaction E in Figure 1. For data collected at 50 and 200 μM PS/POPC membranes, k_c values on the order of k_c (MzII_a formation) were needed to obtain a good description of the data (Table 1). The data obtained at 20 μM lipid were also best described by the three-pathway model (left panel of Figure 7). It is evident from Figure 7 that the channeling hypothesis allowed both the shapes and magnitudes of thrombin, MzII_a, and Pre2 time course curves to be well predicted. The fit of the model to the 50 and 200 μM PL data was insensitive to k_a , because SDS-PAGE could not detect any Pre2 formed under these reaction conditions. Thus, we could estimate only an upper limit to k_a . Surprisingly, this was about the same as estimated in the absence of membranes (Table 1), implying that even optimal membrane concentrations had no amplifying effect on proteolysis of bond Arg²⁷³–Thr²⁷⁴ in prothrombin to form Pre2 and F1.2.

Membrane Origin of the Proposed Channeling Phenomenon. A prediction of the hypothesis outlined above is that it should play a significant role when the surface occupancy of the “effective enzyme” (factor X_a surrounded by a small radius of membrane surface) approaches unity, i.e., when there is little “free” surface from which intermediate would be more likely to escape to solution than to return to factor X_a . The fraction, f , of intermediate that fails to escape this radius of factor X_a influence is thus predicted to decrease with increasing membrane concentration. It is easy to show that $f = k_c/(k_a + k_c + k_c)$, where the k values are pseudo-first-order rate constants for the three possible initial steps of the three-pathway model (Figure 1; Appendix A). Values of f (the “channeling fraction”) calculated in this way are given in Table 1. As predicted, f decreased with increasing membrane concentration from 50 to 2000 μM lipid. Why is channeling reduced at 20 μM membranes when surface occupancy is actually greatest at this membrane concentration (Figure 4B)? The explanation for this is that, at low lipid concentration, there is little free membrane surface available to bind intermediate. Since diffusion of the intermediate on the surface depends on the availability of free surface binding sites, low availability of free surface would increase the probability that intermediate would be released to the solution, thus reducing channeling. Thus, membrane-mediated intermediate channeling will reflect a delicate balance

between surface crowding and surface dilution, explaining the maximum seen at 50 μM lipid. This may offer an explanation for why activated platelets provide PS-exposed membrane surface in terms of small membranous vesicles (19, 39, 40) that would limit the surface area available for enzyme and substrate binding.

Within the context of the channeling hypothesis, $f = 1$ means that all intermediate is channeled to thrombin; none is converted via the traditional parallel-sequential mechanism. This does not mean that activation does not occur via the MzII_a or Pre2 intermediates, just that any intermediate formed is converted to thrombin without being released from the “enzyme”. Viewed in this way, it is clear that even the “best fit” values of the rates of Pre2–F1.2 or MzII_a formation (k_a and k_c) do not represent the total rates of these reactions. They represent only the rates of formation of those intermediates that appear in solution to serve as Michaelis–Menten substrates for the second proteolytic step. According to the channeling hypothesis, a substantial fraction of either intermediate can remain “bound” (i.e., it can return rapidly, via diffusion on the membrane surface, to factor X_a) and is never detected by our steady-state kinetic methods. A similar proposal has been made on the basis of pre-steady-state measurements for prothrombin activation by factor X_a associated with membrane-bound factor V_a (43). Very recently, a study has appeared using much the same approach as employed here to show that bovine factor V_a binding to factor X_a in the absence of membranes causes 39% of intermediate produced to be converted directly to thrombin (2). Our results suggest that, at optimal membrane concentrations, a comparable fraction of intermediate (51%) is channeled to thrombin. It may be that factor V_a and the platelet membrane to which it is bound work together to ensure that the majority of intermediate produced is converted directly to thrombin, thus together accounting for a good portion of the 150000–300000-fold rate enhancement seen for the prothrombinase relative to factor X_a alone (32, 37).

Pathway of Prothrombin Activation in the Presence of Membranes. We used the parameter values summarized in Table 1 to simulate prothrombin activation pathways using the three-step, parallel-sequential model. The results of this simulation are shown in the right panels of Figure 7 in terms of total thrombin formed (solid line) or thrombin formed via MzII_a (small circles) or Pre2 (small triangles) intermediates or via channeling (dashed line). For optimal membrane concentrations (50 and 200 μM), channeling was the major pathway, but we cannot tell from our experiments which intermediate might dominate. For suboptimal (20 μM , protein-crowded surfaces) or excessive (2 mM, diluted surfaces) membrane concentrations, channeling was not essential to explain the data, and we can ask which intermediate dominates activation? At nonoptimal membrane concentrations (20 μM , 2 mM, and to some extent 200 μM), our results indicate that, of the two released intermediates, activation proceeds almost exclusively via MzII_a. In the second paper of this series, we show that a soluble form of PS seems to shut down Pre2 formation and therefore the corresponding pathway.

It is worth noting that the effects of membranes on the rates of the two bond cleavages (Arg³²²–Ile³²³ or Arg²⁷³–Thr²⁷⁴) depend on the substrate for the proteolysis. It has tacitly been assumed that anything that enhanced bond

cleavage in the intermediates should enhance the same bond cleavage in prothrombin (3, 22, 30). Our results indicate that this is not the case for the effect of PS-containing membranes on activation. The rate of Arg³²²–Ile³²³ cleavage was enhanced roughly 10-fold with Pre2 as a substrate (reaction B in Table 2) relative to that with prothrombin as a substrate (reaction C). The most dramatic effect of substrate on membrane-enhanced rate enhancement was for Arg²⁷³–Thr²⁷⁴ cleavage, which was nearly unaffected or even inhibited by membranes with prothrombin as a substrate but was enhanced by 250-fold with MzII_a as a substrate. A 10-fold preference for MzII_a as a substrate, relative to prothrombin, was reported for the enhancement of Arg²⁷⁴–Thr²⁷⁵ (bovine numbering) cleavage by bovine factor X_a with the addition of bovine factor V_a (2). Just as PS-containing membranes and factor V_a seem to have similar effects on channeling, they both seem to favor the MzII_a intermediate. The exact extent to which these two cofactors work together to enhance channeling and to direct activation through MzII_a will be addressed in a later paper.

Even though factor V_a is not present in our reaction, both of the phenomena implied by our observations (channeling and direction of activation via MzII_a) may have physiological significance. According to current views of coagulation, a small amount of thrombin must form on damaged endothelial cells before platelets and factor V can be activated to produce the burst of thrombin that will lead to the platelet plug and ultimately to fibrin to stabilize the clot (35). Our work shows that exposed PS is sufficient to trigger reasonably efficient formation of low levels of thrombin in a membrane-localized fashion.

Effects of Surface Occupancy on Proteolysis. We suggested above that a crowded membrane surface might explain reduced channeling at 20 μM PS/POPC membranes. An interesting feature of this concept of surface crowding is that the degree of channeling and thus the pathway of activation should vary with substrate (prothrombin) concentration. The anomalous substrate dependence of the rate of factor X_a-catalyzed thrombin generation at optimal (50 μM) and suboptimal (20 μM) lipid concentrations (triangles and squares in Figure 5B) may reflect such a shift in pathway. To explain this anomaly, we made the reasonable hypothesis that *f* should vary in proportion to the surface concentration of factor X_a times the surface concentration of free lipid binding sites available to receive surface-diffusing MzII_a:

$$f([\text{II}] = x) = f([\text{II}] = 1 \mu\text{M}) \frac{[\text{PL}(x)]_f [\text{X}_a(x)]_b}{[\text{PL}(1)]_f [\text{X}_a(1)]_b} \quad (1)$$

In this equation, $f([\text{II}] = 1 \mu\text{M})$ was taken as 0.51, as obtained from fitting our data (Table 1); $[\text{PL}]_f$ and $[\text{X}_a]_b$ was obtained as described for Figure 4B. Calculated in this way, the fraction of MzII_a channeled directly to thrombin varied with prothrombin concentration, thereby yielding an anomalous shaped initial rate vs substrate curve (dotted curve in Figure 5B) similar to that observed. We suggest also that the appearance of MzII_a as a released intermediate at high prothrombin concentration during prothrombin activation by the full prothrombinase (36) can be explained by a decrease in the fraction of channeled MzII_a with increasing surface crowding at high prothrombin concentration.

CONCLUSIONS

The purpose of this paper was to define the influence of PS-containing membranes on prothrombin activation in the absence of factor V_a. Our results suggest that PS-containing membranes contribute to prothrombin activation by (1) regulating factor X_a via a dramatic increase in $k_{\text{cat}}/K_{\text{M}}$ (including a decrease in K_{M}) for Arg³²²–Ile³²³ proteolysis, leading either to MzII_a formation or to Pre2 activation, and by a substrate-specific increase in $k_{\text{cat}}/K_{\text{M}}$ for Arg²⁷³–Thr²⁷⁴ proteolysis, leading to MzII_a activation, thus, (2) altering the specificity of factor X_a to favor the meizothrombin intermediate, and (3) channeling the meizothrombin intermediate back to the active site of factor X_a for rapid conversion to thrombin (Table 1). The next paper in this series will ask whether these effects reflect the presence of a membrane surface or of PS molecules.

ACKNOWLEDGMENT

We thank Willem Stevens and Mike Nesheim for guidance with their procedure for isolating bovine Pre2 and F1.2. We acknowledge two anonymous reviewers who put considerable time and thought into comments and suggestions that significantly improved our paper.

APPENDIX

(A) *Analysis of Time Courses of MzII_a, Pre2, and Thrombin Appearance.* (1) *Kinetic Model.* To extract estimates of second-order kinetic constants for Pre2 and MzII_a formation from the three data sets that were collected at any membrane concentration, we modeled prothrombin activation in terms of the two-step, parallel-sequential activation mechanism outlined in Figure 1. For mathematical simplicity, we assumed pseudo-second-order behavior (rate proportional to substrate times enzyme concentration) for all possible reactions of prothrombin activation. In the second-order approximation, the kinetic equations for the appearance and disappearance of the major species in Figure 1 can be expressed as

$$\frac{d[\text{II}](t)}{dt} = -(k_a + k_c + k_e)[\text{II}](t) \quad (\text{A1})$$

$$\frac{d[\text{MzII}_a](t)}{dt} = k_c[\text{II}](t) - k_d[\text{MzII}_a](t) \quad (\text{A2})$$

$$\frac{d[\text{Pre2}](t)}{dt} = k_a[\text{II}](t) - k_b[\text{Pre2}](t) \quad (\text{A3})$$

$$\frac{d[\text{II}_a](t)}{dt} = k_b[\text{Pre2}](t) + k_d[\text{MzII}_a](t) + k_e[\text{II}(t)] \quad (\text{A4})$$

In these expressions, k_a to k_d are first-order rate constants obtained by multiplying the pseudo-second-order constants ($k_{\text{cat}}/K_{\text{M}}$) times the free (for experiments without membranes) or membrane-bound (for experiments with membranes) factor X_a concentration present in a reaction mixture during the activation process. The parameter k_e is the first-order rate constant for direct conversion of prothrombin to thrombin, a process not accounted for by the parallel-sequential model. It was introduced because the parallel-sequential model failed to account for data obtained in the presence of optimal

concentrations of membranes (see Results). Membrane-bound factor X_a concentrations were estimated using the method of Powers and Lentz (34) to solve the linked binding equations. The binding constants used in these calculations are compiled elsewhere (7, 9). This set of linear differential equations has the following set of solutions:

$$[II](t) = [II]_0 e^{-(k_a+k_c+k_e)t} \quad (A1')$$

$$[MzII_a](t) = [II]_0 \frac{k_c}{k_a + k_c + k_e - k_d} (e^{-k_d t} - e^{-(k_a+k_c+k_e)t}) \quad (A2')$$

$$[Pre2](t) = [II]_0 \frac{k_a}{k_a + k_c + k_e - k_b} (e^{-k_b t} - e^{-(k_a+k_c+k_e)t}) \quad (A3')$$

$$[II]_a(t) = [II]_0 - [II](t) - [MzII_a](t) - [Pre2](t) \quad (A4')$$

For reactions C and D of Figure 1, this assumption should be a good approximation since the concentrations of intermediate $MzII_a$ or $Pre2$ did not build to significant levels. The pseudo-second-order assumption makes eqs A1–A4 a set of linear differential equations, which simplifies considerably their solution. Our results show that the assumption of pseudo-second-order kinetics is a good approximation for reactions A and B in Figure 1 only well below 1 μ M prothrombin, a condition that we violate in our experiments. This simplifying assumption can be avoided by replacing k_x by the following expressions for any reaction X:

$$k_x = \frac{k_{cat}^x [X_a]}{K_M^x + [S_x(t)]} \cong \kappa_x [X_a]; \quad \kappa_x = \frac{k_{cat}^x}{K_M^x + [S_x(0)]} \quad (A5)$$

where k_{cat} and K_M are the usual kinetic constants in the Michaelis–Menten formalism and S_x is the substrate of reaction X. This approach requires that one solve a set of nonlinear differential equations, which makes the model mathematically much more difficult. This complication can be avoided by limiting attention in our calculations to times for which $[S(t)] \sim [S(0)]$, i.e., the very initial part of the reaction. In this case, the approximate linear form shown in eq A5 obtains, and k_x in eqs A1–A4 is still independent of substrate concentration for any given experiment, maintaining A1'–A4' as our solutions.

(2) *Global Curve Fitting.* The rate constants k_b and k_d of processes B and D (Figure 1) were obtained by direct DAPA fluorescence assays of $Pre2$ and F1.2 or $MzII_a$ proteolysis by factor X_a in the presence of 25:75 PS/POPC LUV (Table 1). By simultaneously matching calculated values to three data sets (time dependence of $MzII_a$, $Pre2$, and thrombin appearance), we were able to define values for k_a and k_c (Figure 1) resulting in a best fit to the data. The algorithm supplied in the SigmaPlot 2000 package varied k_a and k_c to minimize the sum of squared residuals and fit the calculations to the observed $[Pre2](t)$, $[MzII_a](t)$, and $[II_a](t)$ data.

(B) *Relation of DAPA Fluorescence to $MzII_a$, $Pre2$, and Thrombin Formation.* (1) *Calculation of Expected DAPA Fluorescence Time Course.* Since DAPA binds to all the proteolysis products of prothrombin, the time course of prothrombin proteolysis does not monitor any single aspect of the proteolytic process but rather monitors a complex sum

of events. To model this complex observable, the DAPA fluorescence intensity was expressed as

$$F = \sum_i q_i F_{ib} P_i + q_0 D_f \quad (B1)$$

which can be rearranged to give

$$\frac{F(t) - F(0)}{F(0)} = \sum_i \left(\frac{q_i}{q_0} - 1 \right) \frac{F_{ib} P_i(t)}{D} \quad (B2)$$

in which $F(0)$ is the measured fluorescence intensity at time zero, q_i/q_0 is the fluorescence yield ratio for DAPA bound to peptide i relative to free DAPA (actually a fluorescence efficiency ratio), D is the total DAPA concentration, P_i is the total concentration of peptide i , and F_{ib} is the fraction of peptide i bound to DAPA. In this equation, the sum over i is over all of the protein species that are present and that may contribute to the total DAPA fluorescence (i.e., $MzII_a$, thrombin, and $Pre2$). Our experiments to determine fluorescence yield ratios, as described below, were performed at finite concentrations of protein, and these yield ratios were obtained in ways that correct for background protein fluorescence. However, we also had to correct for background protein fluorescence that occurs in kinetic data sets but not in calculated fluorescence time courses. This was accomplished by multiplying the measured relative fluorescence change (left side of eq B2) by a factor A obtained by comparing the ratio of DAPA fluorescence at the end of proteolysis to that at the beginning of proteolysis to the measured fluorescence yield ratio of thrombin-bound DAPA to unbound DAPA:

$$A = \frac{\frac{q_1}{q_0} F(0) f_b(\infty)}{F(\infty) - F(0)(1 - f_b(\infty))} \quad (B3)$$

Here, q_1/q_0 is the fluorescence yield for DAPA bound to thrombin relative to that of unbound DAPA, $F(0)$ and $F(\infty)$ are the fluorescence intensities at the beginning and end of proteolysis, and $f_b(\infty)$ is the fraction of DAPA bound to thrombin at the completion of prothrombin proteolysis. This approach makes the approximation that the background fluorescence due to activation products at the end of proteolysis will be the same as for the mixture of prothrombin and activation products present during the activation process.

(2) *Equilibrium Distribution of DAPA.* The fractions of proteins bound to DAPA at any given time (F_{ib}) were obtained from the concentrations of activation products (P_i) present at any time. The dissociation constants describing the binding of DAPA to all of the prothrombin proteolysis products (K_{di}) are summarized in Table 2. Since the binding equilibria are linked, an iterative procedure was used to obtain the linked F_{ib} values (fraction of protein species i bound to DAPA) under any set of conditions as expressed in the equations:

$$D_i = D - \sum_i F_{ib} P_i(t) \quad (B4)$$

$$F_{ib} = \frac{P_i + D_i + K_{di} - \sqrt{(P_i + D_i + K_{di})^2 - 4P_i D_i}}{2P_i} \quad (B5)$$

where D_i is the concentration of DAPA bound to the i th protein species and D is the total DAPA concentration (usually 2–5 times the initial prothrombin concentration). During the time course of prothrombin proteolysis, this contribution changes since the concentration of each protein species changes with time. Thus, the fraction of DAPA free and fraction of each protein species bound to DAPA was calculated at each time during the reaction course. In this way, a DAPA fluorescence time course was constructed from observed time courses of MzII_a, II_a, and Pre2 appearance. This could be compared to observed DAPA fluorescence time courses obtained from activity assays and SDS-PAGE as a test of data sets obtained from amidolytic activity assays.

(3) *Determination of q_1/q_0 Values.* For thrombin, the DAPA concentration (D) was kept constant and protein was added, with the fluorescence intensity of the DAPA-protein complex measured after each protein addition being given as

$$F = F_0 + Df_b(q_1 - q_0) + m[\text{II}_a] \quad (\text{B6})$$

where F_0 is the fluorescence intensity in the absence of thrombin when all DAPA is unbound, f_b is the fraction of DAPA bound to protein, and D is the total DAPA concentration. q_1 is the relative fluorescence efficiency of DAPA bound to thrombin, q_0 is the relative fluorescence efficiency of DAPA in solution (taken as 1), and $m[\text{II}_a]$ accounts for background from protein fluorescence. The fraction of DAPA bound is expressed as a function of $[\text{II}_a]$ in terms of the usual quadratic root expression:

$$f_b = \frac{[\text{II}_a] + D_t + K_d - \sqrt{([\text{II}_a] + D_t + K_d)^2 - 4[\text{II}_a]D_t}}{2D_t} \quad (\text{B7})$$

where D_t is the total DAPA concentration. In the limit as $f_b \rightarrow 1$ (i.e., $[\text{II}_a]$ large), this becomes a straight line with slope m and intercept F_∞ , the fluorescence of DAPA bound to thrombin, but free of contributions from background thrombin fluorescence. In the absence of background fluorescence, we may write

$$f_b = \frac{F - F_0}{F_\infty - F_0}; \quad F = D_b q_1 + D_f q_0 \quad (\text{B8})$$

Combining the two expressions in eq B8, we obtain the fluorescence efficiency ratio for thrombin free of the influence of background fluorescence:

$$\frac{q_1}{q_0} = 1 + \frac{F_\infty - F_0}{F_0} \quad (\text{B9})$$

Such a titration could not be performed for Pre2-F1.2, since Pre2 and F1.2 were difficult to obtain in large quantities. Thus, Pre2 concentration was kept constant and different amounts of DAPA were added to the protein solution in a cuvette. In this experiment, the background fluorescence from Pre2-F1.2 was constant and was subtracted from the titration data. DAPA was also added to a second cuvette containing only buffer. The difference in fluorescence intensity between these two cuvettes (ΔF) showed saturable behavior, such that the fraction of Pre2

bound to DAPA (F_b) and the relative fluorescence yield ratio could be obtained according to the expressions:

$$F_b = \frac{\Delta F}{\Delta F_\infty}; \quad \frac{q_3}{q_0} = \frac{\Delta F_\infty}{m_0[\text{Pre2}]} + 1 \quad (\text{B10})$$

where $[\text{Pre2}]$ is the total Pre2 concentration for this experiment, ΔF_∞ is the fluorescence intensity difference at a saturating concentration of DAPA, and m_0 is the slope of the fluorescence intensity versus DAPA concentration in the protein-free sample.

To determine q_2/q_0 for the DAPA-MzII_a complex relative to DAPA in solution, yet a third protocol was needed. Neither of the first two protocols was practical, since isolation of MzII_a was carried out at a DAPA:protein ratio of 5:1 in order to limit MzII_a autolysis (33). The approach used was to measure the fluorescence intensity at a given MzII_a concentration along with the fluorescence intensity (F_0) in the absence of MzII_a. The calculated fractions of DAPA free and bound under these conditions were used to calculate the fluorescence due to DAPA-MzII_a (F), and this was compared to the fluorescence of the same concentration of DAPA in the absence of MzII_a (F_0). The fractions of DAPA free (f_f) and bound were calculated using published binding parameters for MzII_a-DAPA binding (33) and eq B2. DAPA concentration was determined by UV spectrophotometric measurement [$\epsilon^{1\text{mM}}_{330\text{nm}} = 4.01$ (31)]. The fluorescence yield ratio for DAPA-MzII_a was obtained as

$$\frac{q_2}{q_0} = \frac{F - F_0 f_f}{F_0 f_b} \quad (\text{B11})$$

REFERENCES

- Anderson, P. J., and Bock, P. E. (2001) *Anal. Biochem.* 296, 254–261.
- Boskovic, D. S., Bajzar, L. S., and Nesheim, M. E. (2001) *J. Biol. Chem.* 30, 30.
- Boskovic, D. S., Giles, A. R., and Nesheim, M. E. (1990) *J. Biol. Chem.* 265, 10497–10505.
- Carlisle, T. L., Bock, P. E., and Jackson, C. M. (1990) *J. Biol. Chem.* 265, 22044–22055.
- Chase, T., Jr., and Shaw, E. (1970) in *Methods in Enzymology* (Perlemann, G. E., and Lorand, L., Eds.) pp 20–27, Academic Press, New York.
- Chen, P. S., Jr., Toribara, T. Y., and Warner, H. (1956) *Anal. Chem.* 28, 1756–1758.
- Chen, Q., and Lentz, B. R. (1997) *Biochemistry* 36, 4701–4711.
- Chrumbach, A., Jovin, T. M., Svendsen, P. J., and Rodbard, D. (1976) in *Methods of Protein Separation* (Catsimpoulus, N., Ed.) pp 27–144, Plenum Press, New York.
- Cutsforth, G. A., Whitaker, R. N., Hermans, J., and Lentz, B. R. (1989) *Biochemistry* 28, 7453–7461.
- Di Scipio, R. G., Hermodson, M. A., Yates, S. G., and Davie, E. W. (1977) *Biochemistry* 16, 698–706.
- Downing, M. R., Butkowski, R. J., Clark, M. M., and Mann, K. G. (1975) *J. Biol. Chem.* 250, 8897–8906.
- Esmon, C. T., and Jackson, C. M. (1974) *J. Biol. Chem.* 249, 7791–7797.
- Fenton, J. W. D. (1981) *Ann. N.Y. Acad. Sci.* 370, 468–495.
- Hibbard, L. S., Nesheim, M. E., and Mann, K. G. (1982) *Biochemistry* 21, 2285–2292.
- Husten, E. J., Esmon, C. T., and Johnson, A. E. (1987) *J. Biol. Chem.* 262, 12953–12961.
- Jackson, C. M., and Nemerson, Y. (1980) *Annu. Rev. Biochem.* 49, 765–811.

17. Jameson, G. W., Roberts, D. V., Adams, R. W., Kyle, W. S., and Elmore, D. T. (1973) *Biochem. J.* 131, 107–117.
18. Jesty, J., and Nemerson, Y. (1976) *Methods Enzymol.* 45, 95–107.
19. Jones, M. E., Lentz, B. R., Dombrose, F. A., and Sandberg, H. (1985) *Thromb. Res.* 39, 711–724.
20. Koppaka, V., Wang, J., Banerjee, M., and Lentz, B. R. (1996) *Biochemistry* 35, 7482–7491.
21. Krishnaswamy, S., Church, W. R., Nesheim, M. E., and Mann, K. G. (1987) *J. Biol. Chem.* 262, 3291–3299.
22. Krishnaswamy, S., Mann, K. G., and Nesheim, M. E. (1986) *J. Biol. Chem.* 261, 8977–8984.
23. Lentz, B. R., Wu, J. R., Sorrentino, A. M., and Carleton, J. N. (1991) *Biophys. J.* 60, 942–951.
24. Mann, K. G. (1976) *Methods Enzymol.* 45, 123–156.
25. Mann, K. G., Elion, J., Butkowski, R. J., Downing, M., and Nesheim, M. E. (1981) *Methods Enzymol.* 80, 286–302.
26. Markwell, M. A. (1982) *Anal. Biochem.* 125, 427–432.
27. Mayer, L. D., Hope, M. J., and Cullis, P. R. (1986) *Biochim. Biophys. Acta* 858, 161–168.
28. Mitra, P., Pal, A. K., Basu, D., and Hati, R. N. (1994) *Anal. Biochem.* 223, 327–329.
29. Myrnel, K. H., Lundblad, R. L., and Mann, K. G. (1976) *Biochemistry* 15, 1767–1773.
30. Nesheim, M. E., and Mann, K. G. (1983) *J. Biol. Chem.* 258, 5386–5391.
31. Nesheim, M. E., Prendergast, F. G., and Mann, K. G. (1979) *Biochemistry* 18, 996–1003.
32. Nesheim, M. E., Taswell, J. B., and Mann, K. G. (1979) *J. Biol. Chem.* 254, 10952–10962.
33. Pei, G., and Lentz, B. R. (1991) *Blood Coagulation Fibrinolysis* 2, 309–316.
34. Powers, D. D., and Lentz, B. R. (1993) *J. Biol. Chem.* 268, 3234–3237.
35. Roberts, H. R., Monroe, D. M., and Hoffman, M. (2000) in *Williams Hematology* (Beutler, E., Lichtman, M. A., Coller, B. S., Kipps, T. J., and Seligsohn, U., Eds.) 6th ed., Chapter 112, pp 1409–1434, McGraw-Hill, New York.
36. Rosing, J., and Tans, G. (1988) *Thromb. Haemostasis* 60, 355–360.
37. Rosing, J., Tans, G., Govers-Riemslog, J., Zwaal, R., and Hemker, H. (1980) *J. Biol. Chem.* 255, 274–283.
38. Rosing, J., Zwaal, R. F., and Tans, G. (1986) *J. Biol. Chem.* 261, 4224–4228.
39. Sandberg, H., Bode, A. P., Dombrose, F. A., Hoehli, M., and Lentz, B. R. (1985) *Thromb. Res.* 39, 63–79.
40. Sims, P. J., Faioni, E. M., Wiedmer, T., and Shattil, S. J. (1988) *J. Biol. Chem.* 263, 18205–18212.
41. Stevens, W. K., and Nesheim, M. E. (1993) *Biochemistry* 32, 2787–2794.
42. Swanstrom, R., and Shank, P. R. (1978) *Anal. Biochem.* 86, 184–92.
43. Walker, R. K., and Krishnaswamy, S. (1994) *J. Biol. Chem.* 269, 27441–27450.
44. Wang, J., Majumder, R., and Lentz, B. R. (2001) *Biophys. J.* (submitted for publication).
45. Wu, J. R., and Lentz, B. R. (1994) *Thromb. Haemostasis* 71, 596–604.
46. Wyckoff, M., Rodbard, D., and Chrambach, A. (1977) *Anal. Biochem.* 78, 459–482.

BI0116893